Pulse-Modulated Control Synthesis for a Flexible Spacecraft

Tobin C. Anthony* and Bong Wie†
University of Texas at Austin, Austin, Texas 78713
and
Stanley Carroll‡
NASA Marshall Space Flight Center, Huntsville, Alabama 35812

The describing function method is employed for the nonlinear control analysis and design of a flexible spacecraft equipped with pulse-modulated reaction jets. The method provides a means of characterizing the pulse modulator in terms of its gain and phase for structural mode limit-cycle analysis. Although the describing function method is inherently inexact and is not widely used in practice, a new way of utilizing it for practical control design problems is presented. It is shown that the approximations inherent in the method can be accounted for as a modeling uncertainty for the nonlinear control robustness analysis. The pulse-modulated control system of the INTELSAT 5 spacecraft is used as an example to illustrate the concept and methodology developed in the paper. The nonlinear stability margins predicted by the describing function analysis are verified from nonlinear simulations.

Introduction

STRUCTURAL mode interaction with reaction jet control systems is a primary concern for the design of future large spacecraft, including the space station. The nonlinear control instability in such systems appears in the form of a structural mode limit cycle caused by thruster chatterings at the structural mode frequency. Although considerable attention has been directed toward the control-structure interaction problems of large space structures, the nonlinear control interaction with flexible modes has not been extensively investigated.

In this paper, a frequency-domain approach is developed for the design of a pulse-modulated nonlinear control system of a flexible spacecraft. The approach involves the use of the well-known describing function method, also known as the harmonic balance method,[1-3] which is basically a frequency-response technique used primarily to predict limit cycling of nonlinear systems. Within the last several decades, many researchers have attempted to improve the accuracy of the describing function method by establishing new criteria to approximate the output of a nonlinear device; despite their efforts, the results are not much used in practice. The reason is, in part, that the describing function method is inherently inexact and represents only a first-order approximation of the gain and phase characteristics of a nonlinear device.

This paper, however, presents a new way to use the describing function method for designing nonlinear control systems. Analogs of the classical concept of gain/phase margins are applied to nonlinear systems to designate nonlinear stability margins; these margins give the designer a means of measuring the limit-cycling tendency of a control system. The approximations inherent in the method are interpreted as a modeling uncertainty for designating the nonlinear stability margins. The describing function method is not employed here as a means of accurately predicting limit-cycling information; instead, it is used as a method for characterizing a nonlinear component in terms of its gain and phase. In most cases, the control designer is more interested in determining whether the system will limit cycle as opposed to accurately identifying the oscillation characteristics (e.g., limit-cycle frequency and amplitude).

Once the pulse modulator is adequately characterized by the describing function, the designer can iteratively synthesize a linear compensator and/or pulse modulator such that sufficient margins, with respect to limit-cycling condition, are attained. The proposed concept and methodology are applied to the design example of the INTELSAT 5 spacecraft equipped with a reaction jet attitude-control system. The interaction of the spacecraft's flexible solar arrays with the pulse modulator has been a major concern.[4,5] Such interaction appears in the form of structural mode limit cycling. Control design examples for the INTELSAT 5 spacecraft are presented in order to illustrate the usefulness of the concept and methodology in avoiding the structural model limit cycling.

Pulse Modulation

Pulse modulation represents the control logic behind reaction jet control systems of various spacecraft. Unlike other actuators, such as reaction wheels, thruster output consists of two values: on or off. Proportional thrusters, whose fuel valves open a distance proportional to the commanded thrust level, are not employed in practice. Mechanical considerations prohibit proportional valve operation largely because of dirt particles, which prevent complete closure for small valve openings; fuel leakage through the valves consequently produces opposing thruster firings. Pulse-modulation techniques have been developed that fully open and close the fuel valves while producing a nearly linear duty cycle. In general, pulse modulators produce a pulse command sequence to the

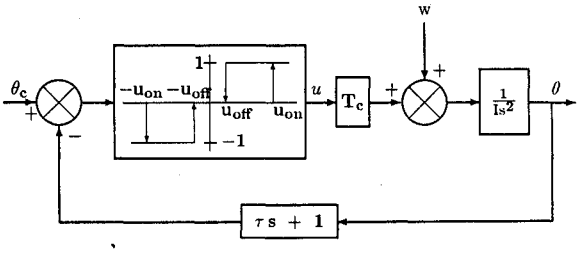

Fig. 1 Spacecraft on-off control system with Schmitt trigger.

Received March 20, 1989; revision received June 23, 1989; presented as Paper 89-3433 at the AIAA Guidance, Navigation, and Control Conference, Boston, MA, Aug. 14-16, 1989.

*Graduate Research Assistant; also, Aerospace Engineer, NASA Goddard Space Flight Center. Member AIAA.

†Assistant Professor, Dept. of Aerospace Engineering and Engineering Mechanics; currently, Associate Professor, Department of Mechanical and Aerospace Engineering, Arizona State University, Tempe, AZ. Member AIAA.

‡Aerospace Engineer, Control Systems Division.

thruster valves by adjusting the pulse width and/or pulse frequency.

Several commonly used, flight-proven pulse modulators are discussed in this section. Brief descriptions and static characteristics are given for each modulator. The pulse frequency of these modulators is usually fast compared to the spacecraft attitude-control bandwidth, and the static characteristics are often used for the modulator design.

Schmitt Trigger

Strictly speaking, this device, which is often called a relay with deadband/hysteresis, is not a pulse modulator. A phase-plane controller that is basically Schmitt trigger logic is used on the Space Shuttle reaction control system (RCS).[6] The advantage of this device, as opposed to other pulse modulators, is its simplicity. A disadvantage of the Schmitt trigger is the dependence of its static characteristics on the spacecraft inertia. The schematic shown in Fig. 1 depicts a simple rigid spacecraft attitude-control system. The equation of motion for the spacecraft is simply given by

$$I\ddot{\theta} = T_c u + w \tag{1}$$

where

I = spacecraft inertia, kg m^2
u = Schmitt trigger output, 0 or ± 1
T_c = control torque level, Nm
w = disturbance torque, Nm

The rigid-body limit-cycling characteristics of this system can be obtained as in Ref. 7,

$$\Delta = \frac{Ih}{\tau T_c} \tag{2}$$

$$A = \frac{T_c(u_{on} + u_{off})}{2} + \frac{I^2h^2}{8\tau} \tag{3}$$

$$P = 4\tau\left(\frac{u_{on} + u_{off}}{h} + \frac{Ih}{2\tau^2}\right) \tag{4}$$

where

$h \triangleq u_{on} - u_{off}$

τ = switching line slope

Also, Δ is defined as the Schmitt trigger minimum pulse width, A the limit-cycle amplitude, and P the limit-cycle period. Note that the Schmitt trigger minimum pulse width depends on spacecraft parameters: the spacecraft inertia and thrust level. These parameters tend to change over time; as a result, the minimum pulse width will vary as well. Knowledge of the spacecraft properties is therefore required to determine the thruster minimum pulse width.

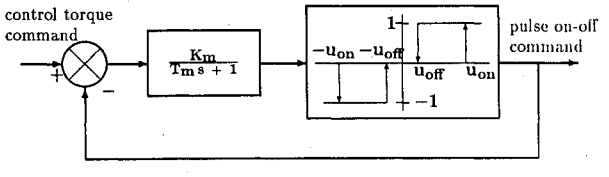

Fig. 2 PWPF modulator.

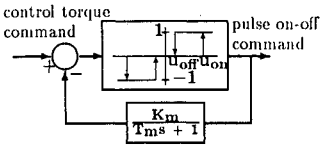

Fig. 3 Derived-rate modulator.

Pulse-Width Pulse-Frequency Modulator

The pulse-width pulse-frequency (PWPF) modulator has been used in the control systems of such spacecraft as the Agena satellite,[8] INTELSAT 5, INSAT, and ARABSAT.[5] The device, as shown in Fig. 2, comprises chiefly two components: a first-order lag filter and a Schmitt trigger inside a feedback loop. With a constant input, the PWPF modulator drives the thruster valve with an on-off pulse sequence having a nearly linear duty cycle with the input amplitude. The duty-cycle or modulation factor is defined as the average output of the modulator. The static characteristics of the PWPF modulator are summarized as follows:

$$T_{on} = -T_m \ell n\left\{\frac{(1-h)E_d - (E-1)}{E_d - (E-1)}\right\} \tag{5}$$

$$T_{off} = -T_m \ell n\left\{\frac{E_d - E}{(1-h)E_d - E}\right\} \tag{6}$$

$$f = \frac{1}{T_{on} + T_{off}} \tag{7}$$

$$\Delta = -T_m \ell n\left(1 - \frac{h}{K_m}\right) \approx \frac{hT_m}{K_m} \tag{8}$$

where T_{on} is the thruster pulse width, T_{off} the thruster off-time, f the pulse frequency, and E the static input magnitude; $E_d = u_{on}/K_m$, which is the equivalent internal deadband, and the duty cycle is given by fT_{on}.

In contrast to the Schmitt trigger, the static characteristics of the PWPF modulator are independent of the spacecraft inertia because of the feedback loop within the device. The presence of the filter and the feedback loop, however, inhibits linear analysis of the device's dynamic characteristics.

Derived-Rate Modulator

The derived-rate and PWPF modulators are similar in format, as seen in Fig. 3, except that the first-order filter now compensates the Schmitt trigger output in the feedback path. The device is used in much the same way as the PWPF modulator except that the derived-rate modulator introduces phase lead into a system as opposed to the PWPF modulator, which is a phase-lag device. The static characteristics, shown here, are similar to the PWPF modulator:

$$T_{on} = -T_m \ell n\left\{1 - \frac{h}{K_m u_m - (E - u_{on})}\right\} \tag{9}$$

$$T_{off} = T_m \ell n\left(1 + \frac{h}{E - u_{on}}\right) \tag{10}$$

$$f = \frac{1}{T_{on} + T_{off}} \tag{11}$$

$$\Delta \approx \frac{hT_m}{K_m} \tag{12}$$

where the duty cycle is given by fT_{on}. The derived-rate modulator is as difficult as the PWPF modulator to analyze in a limit-cycling situation. As a result, the describing function method may be employed to characterize the modulator in terms of its gain and phase.

Pulse-Width Modulator

The pulse-width modulator (PWM) differs from the modulators discussed previously in that it is essentially a discrete-time device; the PWPF and derived-rate modulators can be digitally implemented but are usually analyzed as continuous-time systems. The PWM, shown in Fig. 4, is to be used in the orbital maneuvering vehicle RCS.[9]

The output of this particular device is not a thruster firing state as in the previously described devices; instead, the PWM output is thruster pulse width. A zero-order-hold (ZOH)

device transmits that signal to the thrusters. The value d_1 represents the minimum pulse width of the system; this deadzone is directly proportional to the attitude deadband. The value d_2 represents the maximum pulse width of the RCS; it is equivalent to the microprocessor sampling period. As a result, the pulse frequency and the minimum pulse width of the modulator are fixed; a thruster firing command is given during every microprocessor sampling period even if the pulse is of zero width.

The delay in the feedback loop introduces damping to the system; maximum damping occurs when the feedback signal is smaller than the PWM input. If the input signal is not greater than the feedback signal, the modulator may limit cycle itself. This criterion enables the designer to determine the feedback gain K_f. The feedforward gain K_d is selected as a result of the minimum pulse criterion.

Describing Function Analysis for Pulse Modulators

A proper selection of the modulator parameters, based on its static characteristics, does not guarantee the closed-loop stability of the control system. The pulse modulator, being a nonlinear device, cannot be adequately analyzed through the application of linear analysis techniques. Still, the designer must be concerned about linear compensator design, linear/nonlinear stability margins, and structural mode limit cycling. These problems can be approached by using the describing function method to characterize the pulse modulator in terms of its gain and phase.

In the describing function analysis, it is assumed that the fundamental harmonic component of the output is significant when the input to a nonlinear element is sinusoidal. The describing function of a nonlinear element is then defined to be the complex ratio of the fundamental harmonic component of the output to the input sinusoid; that is,

$$N(X,\omega) = (Y_1/X)e^{j\phi} \tag{13}$$

where

N = describing function
X = sinusoidal input amplitude
ω = frequency of input sinusoid
Y_1 = amplitude of the fundamental harmonic
Y_1/X = describing function gain
ϕ = describing function phase

Calculation of the describing function involves a conventional Fourier series analysis to obtain the fundamental component of the output. Y_1 and ϕ may then be expressed as

$$Y_1 = \sqrt{A_1^2 + B_1^2} \tag{14}$$

$$\phi = \tan^{-1}(A_1/B_1) \tag{15}$$

where

$$A_1 = \frac{1}{\pi}\int_0^{2\pi} y(t)\cos(\omega t)\mathrm{d}(\omega t) \tag{16}$$

$$B_1 = \frac{1}{\pi}\int_0^{2\pi} y(t)\sin(\omega t)\mathrm{d}(\omega t) \tag{17}$$

$y(t)$ = output of the nonlinear device

If the nonlinear element can be adequately characterized by the describing function $N(X,\omega)$, the loop transfer function of a negative feedback control system is simply given by $N(X,\omega)G(j\omega)$, where $G(j\omega)$ is the frequency-response function of the linear components of the loop. Thus, the study of limit-cycle stability involves an investigation of the following equation:

$$1 + N(X,\omega)G(j\omega) = 0 \tag{18}$$

or

$$G(j\omega) = -1/N(X,\omega) \tag{19}$$

Equation (19) is often called the harmonic balance equation. The main advantage of the describing function method using Eq. (19) is its simplicity. For example, we simply plot the $-1/N$ locus and the $G(j\omega)$ locus. If two loci intersect, the system may exhibit a limit cycle, which is characterized by the amplitude X and frequency ω. Note that the amplitude and frequency of the limit cycle indicated by the intersection of $-1/N$ locus and $G(j\omega)$ locus are approximate values. Furthermore, if they intersect tangentially, the system may not actually exhibit a limit cycle.

Figure 5 shows a $-1/N(X,\omega)$ locus for a PWPF modulator in the gain-phase plane. Because the modulator describing function is dependent on ω, a limit cycle occurs only if the frequencies of the two curves are equivalent at the intersection point.

The INCA program was used to create the $-1/N(X,\omega)$ locus in Fig. 5.[10] INCA has been enhanced to allow the calculation of describing functions as well as inclusion of the $-1/N(X,\omega)$ locus in the frequency domain as in Fig. 5. To calculate describing functions for devices such as the PWPF modulator for which the describing function cannot be expressed analytically, INCA solves Eqs. (16) and (17) for steady-state output. All of the $-1/N(X,\omega)$ loci in this paper were constructed using the enhanced INCA software.

The describing function of the modulator is made up of two components: 1) the minimum-amplitude line, the vertical line on the right side of the curve set, and 2) the roughly horizontal lines that constitute the $-1/N(X,\omega)$ loci for different values of frequency. The constant-frequency lines are a function of amplitude X. In the INCA program, these curves are calculated, for a given input amplitude, only as long as the modulator output contains just two opposing pulses with a

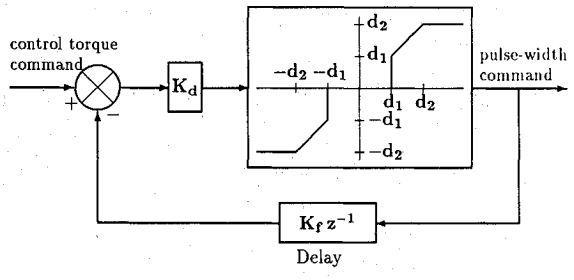

Fig. 4 Pulse-width modulator.

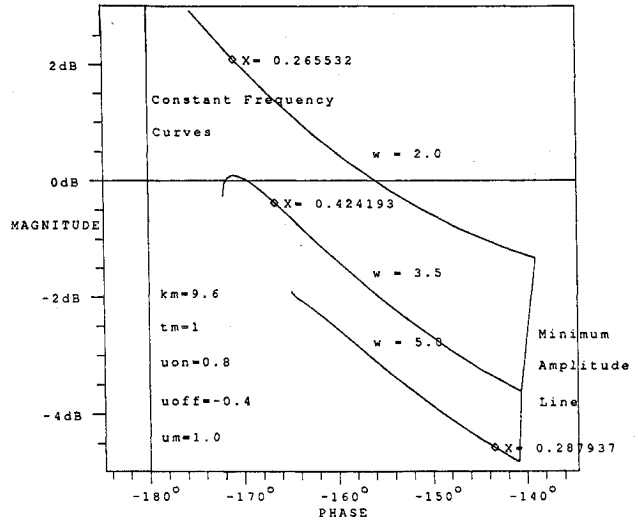

Fig. 5 $-1/N(X,\omega)$ loci for the PWPF modulator.

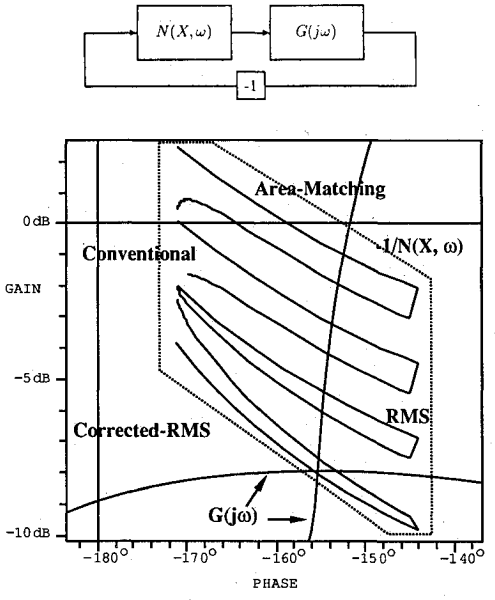

Fig. 6 PWPF modulator region of uncertainty for $-1/N(X,\omega)$ loci.

frequency ω. When the input amplitude is increased, the width of each output increases until a point is reached at which the modulator produces more than two opposing pulses per cycle. These extraneous pulses prevent meaningful representation of the modulator output with a single harmonic sinusoid. As a result, all discussions of PWPF modulator describing functions in this paper refer to single-pulse output.

The describing function method is most useful when a realistic sinusoidal model of the pulse output is used to determine gain and phase change of a nonlinear device. It is difficult, however, to determine a criterion that best represents the pulse output in sinusoidal form. A popular representation is the fundamental harmonic of a Fourier series. However, the fundamental Fourier harmonic is only the first term of an infinite-order series. It is difficult to consider the fundamental Fourier harmonic the best approximation without acknowledging the contribution of the higher harmonics.

The gain and phase characteristics of a describing function depend on the method defined to approximate the periodic nonlinear output with a sinusoid of the same frequency. Several other types of describing function methods have been proposed in the literature. A method that is treated in this paper involves approximating the modulator pulse signal with a sine curve of equal area. The first integral of torque with respect to time is total angular momentum; therefore, two torque profiles of equal area will impart identical impulses to a linear plant.

Calculation of the area-matching describing function for the PWPF modulator is computationally simple. The area of a modulator pulse A_p, integrated from 0 to π/ω, is simply Δ, where Δ is defined as the modulator output pulse width. The area of a sine curve over the same period is $2Y_s/\omega$, where Y_s is the area-matching sinusoid amplitude and ω is the frequency of both the sinusoid and pulse signal. Equating these two relations yields

$$Y_s = \frac{\omega\Delta}{2} \tag{20}$$

The amplitude of the Fourier fundamental harmonic Y_1 can be found by solving Eqs. (16) and (17) and substituting into Eq. (14):

$$Y_1 = \frac{4}{\pi}\sin\left(\frac{\omega\Delta}{2}\right) = \frac{4}{\pi}\sin(Y_s) \tag{21}$$

Equation (21) states that for small values of Y_s, Y_1 differs from Y_s by a factor of 2.1 dB, as displayed in Fig. 6. This value can be interpreted as the uncertainty of the actual modulator gain. The modulator gain obviously depends on the criteria used to treat the output signal. As a result, the designer can utilize a region of gain uncertainty, instead of a single $-1/N(X,\omega)$ locus, to evaluate the limit-cycling tendency.

Another approximation method[11] also involves sinusoidal input to the nonlinear device. Similarly to the area-matching technique, the root-mean-square (rms) describing function method expresses the gain of a pulse-modulating device as a function of the pulse area. It has been used in evaluation of systems that contain odd-valued nonlinear devices.

In this procedure, the curve-approximating criterion specifies that the sinusoidal output have the same rms value as the actual modulator ouput. This is similar to Eqs. (14–17) in that the describing function gain $|N(X,\omega)_{\text{rms}}|$ is defined as

$$|N(X,\omega)_{\text{rms}}| = \sqrt{\frac{\int_0^{2\pi}[y(t)]^2\,d\omega t}{\int_0^{2\pi}[X\sin(\omega t)]^2\,d\omega t}} \tag{22}$$

For a pulsed output, the amplitude of the output sinusoid is

$$Y_{\text{rms}} = \sqrt{\frac{2\omega\Delta}{\pi}} \tag{23}$$

Note that the rms output sinusoidal amplitude is greater than that of the area-matching and fundamental harmonic approximations; the reason is that $Y_{\text{rms}} > Y_1$ for $\omega\,\Delta < 1$. In fact, for small values of $\omega\,\Delta$, such that $\sin(\omega\Delta) \approx \omega\,\Delta$, $Y_1 = 2Y_{\text{rms}}^2$.

For non-pulse-modulated systems, it can be difficult to evaluate the numerator of the right-hand side of Eq. (22). If $y(t)$ is assumed to be the superposition of an infinite number of harmonics, the evaluation of the equation is formidable. For example, Eq. (22) would be evaluated as

$$|N(X,\omega)_{\text{rms}}| = \frac{\sqrt{Y_1^2 + Y_3^2 + Y_5^2 + \cdots + Y_{2n-1}^2 + \cdots}}{X} \tag{24}$$

or

$$Y_{\text{rms}} = \sqrt{Y_1^2 + Y_3^2 + Y_5^2 + \cdots + Y_{2n-1}^2 + \cdots} \tag{25}$$

where Y_{2n-1} represents amplitude of the odd Fourier harmonics. As a result, some authors have employed a corrected rms describing function method based on the rms approximation. In this technique, only the first two odd harmonics are used in evaluation of a describing function. As a result, the corrected rms describing function is expressed as

$$|N(X,\omega)_{c-\text{rms}}| = \frac{\sqrt{Y_1^2 + Y_3^2}}{X} \tag{26}$$

where

$$Y_1 = \frac{4}{\pi}\sin\left(\frac{\omega\Delta}{2}\right)$$

$$Y_3 = \frac{4}{3\pi}\sin\left(\frac{3\omega\Delta}{2}\right)$$

From inspection of Eq. (26), it is obvious that $Y_{c-\text{rms}} < Y_{\text{rms}}$.

As mentioned previously, evaluation of the pulse-modulator gain is not accomplished accurately using the describing function method. Table 1 summarizes the different gain approximations of a pulse-modulator output. There are valid

Table 1 Describing function amplitude comparison

Describing function method	Sinusoidal amplitude
Conventional	$Y_1 = \frac{4}{\pi}\sin\left(\frac{\omega\Delta}{2}\right)$
Area-matching	$Y_s = \frac{\omega\Delta}{2}$
Root-mean-square (rms)	$Y_{\text{rms}} = \sqrt{\frac{2\omega\Delta}{\pi}}$
Corrected rms	$Y_{c-\text{rms}} = \frac{4}{\pi}\sqrt{\sin^2\left(\frac{\omega\Delta}{2}\right) + \frac{1}{9}\sin^2\left(\frac{3\omega\Delta}{2}\right)}$

physical justifications for the use of each of the different modeling methods. The fundamental flaw in each procedure, however, is the necessity to approximate a discontinuous pulse signal with a single-harmonic sine wave. This is the feature of describing function theory that inhibits its usefulness in accurately predicting limit-cycle behavior.

The describing function phase can be obtained directly from Eq. (15). Because INCA calculates only output containing two pulses per cycle, the phase lag of the Fourier sinusoid exactly matches that of the modulator output. This analogy is not readily evident when the modulator produces multiple pulses per cycle; in this situation, the pulses often occur irregularly throughout the firing period prohibiting any evaluation of describing function phase.

Figure 6 represents an evaluation of the modeling methods for a PWPF modulator discussed earlier. As displayed in the figure, the disparity in location of the curves is evidence of the disagreement of the methods outlined in Table 1. What is important to realize is that the methods are in relative agreement; they all lie wihtin a few decibels of one another. As a result, the different values of gain describe a region on the Nichols plot that is depicted in Fig. 6. If it is acknowledged that the approximation methods presented in Table 1 have some physical justification, the dashed area can be referred to as a region of describing function uncertainty. This region can be defined on the Nichols plot, which loosely designates the modulator's $-1/N(X,\omega)$ locus. Instead of using this information to predict limit-cycle behavior, the designer can use this plot to measure a control system's tendency to limit cycle. In practical cases, avoidance of the limit cycle is more important than predicting its oscillation characteristics.

A system whose $G(j\omega)$ locus passes through this region has a greater chance of exhibiting a sustained oscillation. It is apparent that the actual boundaries of the region depend on the parameters of the pulse modulator. The describing function uncertainty region is only an approximation in itself; uncertainties in modeling the pulse modulator prevent any confidence in the gain boundaries. Therefore, a system whose frequency response is horizontal in the vicinity of the $-1/N(X,\omega)$ locus has a smaller chance of actually passing through the region; these systems tend not to experience limit cycles. Conversely, frequency-response curves that are nearly vertical in the vicinity of the gain uncertainty region tend to experience limit-cycle oscillation. This phenomenon is depicted in Fig. 6.

As a result, the describing function uncertainty region can be a useful tool in robust compensation design for pulse-modulated control systems. A designer can synthesize linear compensation such that the $G(j\omega)$ locus avoids the uncertainty region of $-1/N(X,\omega)$ locus as much as possible.

Nonlinear Control Design Methodology

The design methodology presented in this section employs the describing function method to characterize a nonlinear element in terms of its gain and phase. The conventional describing function analysis emphasizes an accurate prediction of the limit-cycle amplitude and frequency. The control system designer, however, is more concerned with the avoidance of the limit cycle than its accurate analysis. A methodology is developed here to aid the control designer in avoiding repetitive computer simulation in the process of pulse-modulated control system design.

The following six steps can be used as a guideline for on-off control system design for flexible spacecraft.

1) *Rigid-body mode stabilization*: For this step, the effect of the pulse modulator on the system is ignored. The type of compensation for rigid-body mode control depends on the control bandwidth or settling time requirement. In general, a phase-lead filter is used when direct rate feedback is not possible. The pole and zero locations of the phase-lead filter should be chosen properly in order to attenuate high-frequency noise.

2) *Pulse-modulator synthesis*: Usually, the type of pulse modulator is fixed as a result of previous spacecraft design. Certain factors that must be considered in the modulator design include ease of hardware/software implementation, stabilization requirements of flexible modes, and the modula-

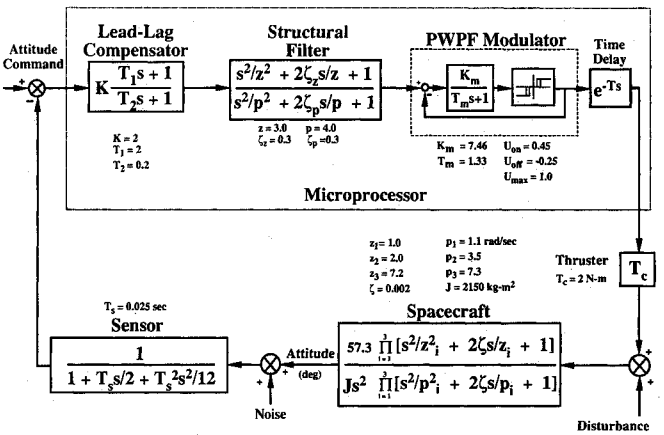

Fig. 7 Flexible spacecraft attitude-control system.

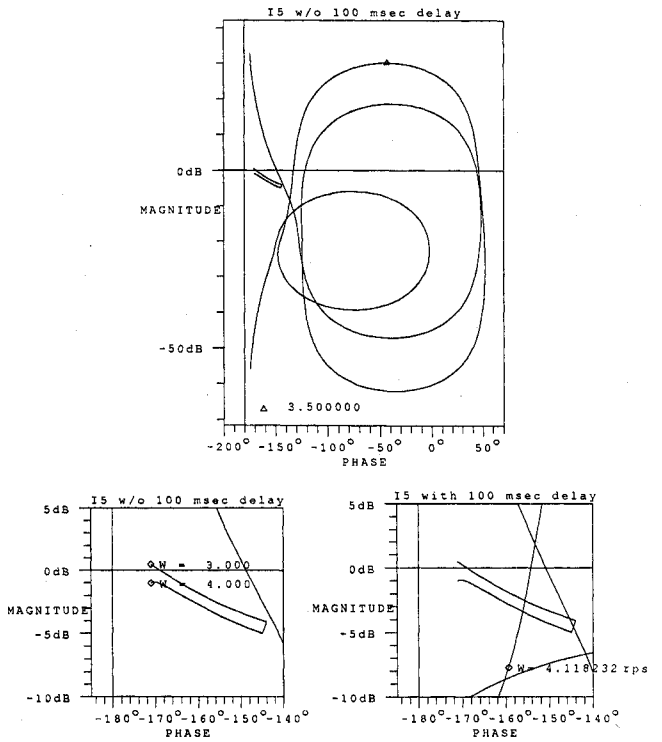

Fig. 8 Case 1 describing function analysis.

tor static characteristics (i.e., minimum pulse width, duty cycle).

3) *Linear analysis and structural mode stabilization*: By neglecting the presence of the pulse modulator, linear analysis methods such as root locus and frequency response enable the control designer to investigate the linear stability of the flexible modes. Higher-order filters may be necessary, in addition to the rigid-body mode controller, to compensate for unstable flexible modes.

4) *Describing function analysis*: Gain and phase characteristics of the nonlinear controller can be obtained through the describing function method. The effects of the linear compensation developed in step 3 can be evaluated by observation of the proximity of the $-1/N(X,\omega)$ and the $G(j\omega)$ loci. By employing describing function analysis, further linear stabilization can be developed, in an iterative manner, which will provide sufficient separation between the two loci in the frequency domain; this separation will insure robustness of the system in terms of structural limit cycling. This technique gives the designer a feeling for the system's tendency toward limit cycling, something that nonlinear simulations do not do.

5) *Nonlinear simulation*: The results in step 4 can be verified by a numerical simulation. The existence of a structural mode limit cycle, as well as approximate nonlinear stability margins, can be verified in this step.

6) *Linear analysis iteration*: If the designer is not satisfied with nonlinear stability margins or the possibility of limit cycling, the design process can be repeated from step 3 by altering or adding to the linear compensation. If needed, the pulse modulator itself can be modified to further increase the nonlinear stability margins.

Table 2 Compensator parameters

	Rigid-body controller	Structural filter
Case 1	$T_1 = 2$ $T_2 = 0.2$	N/A
Case 2	$T_1 = 2$ $T_2 = 0.2$	$z = 3.0$ $\zeta_z = 0.3$ $p = 4.0$ $\zeta_p = 0.3$
Case 3	$T_1 = 2$ $T_2 = 0.2$	$z = 3.4$ $\zeta_z = 0.002$ $p = 3.4$ $\zeta_p = 1$
Case 4	$T_1 = 2$ $T_2 = 0.2$	$z = 3.6$ $\zeta_z = 0.002$ $p = 3.6$ $\zeta_p = 1$

Applications of Computer-Aided Design

A generic example of a nonlinear control system of flexible spacecraft, shown in Fig. 7, is investigated here to demonstrate the concept and methodology developed in the paper. The control system consists of three elements: the flexible spacecraft, the attitude sensor, and the controller. The sensor is modeled as a sample and ZOH device that introduces phase lag into the control loop. The controller is composed of linear compensation and a pulse-modulation logic. The linear compensation consists of a phase-lead filter for rigid-body mode stabilization and a structural filter for flexible mode compensation.

Except for the structural filter and digital control implementation, the control system parameters are derived from the INTELSAT 5 yaw axis control system[4]; however, most spacecraft with digital control systems can be represented in this format. A nonlinear instability, which can arise from the

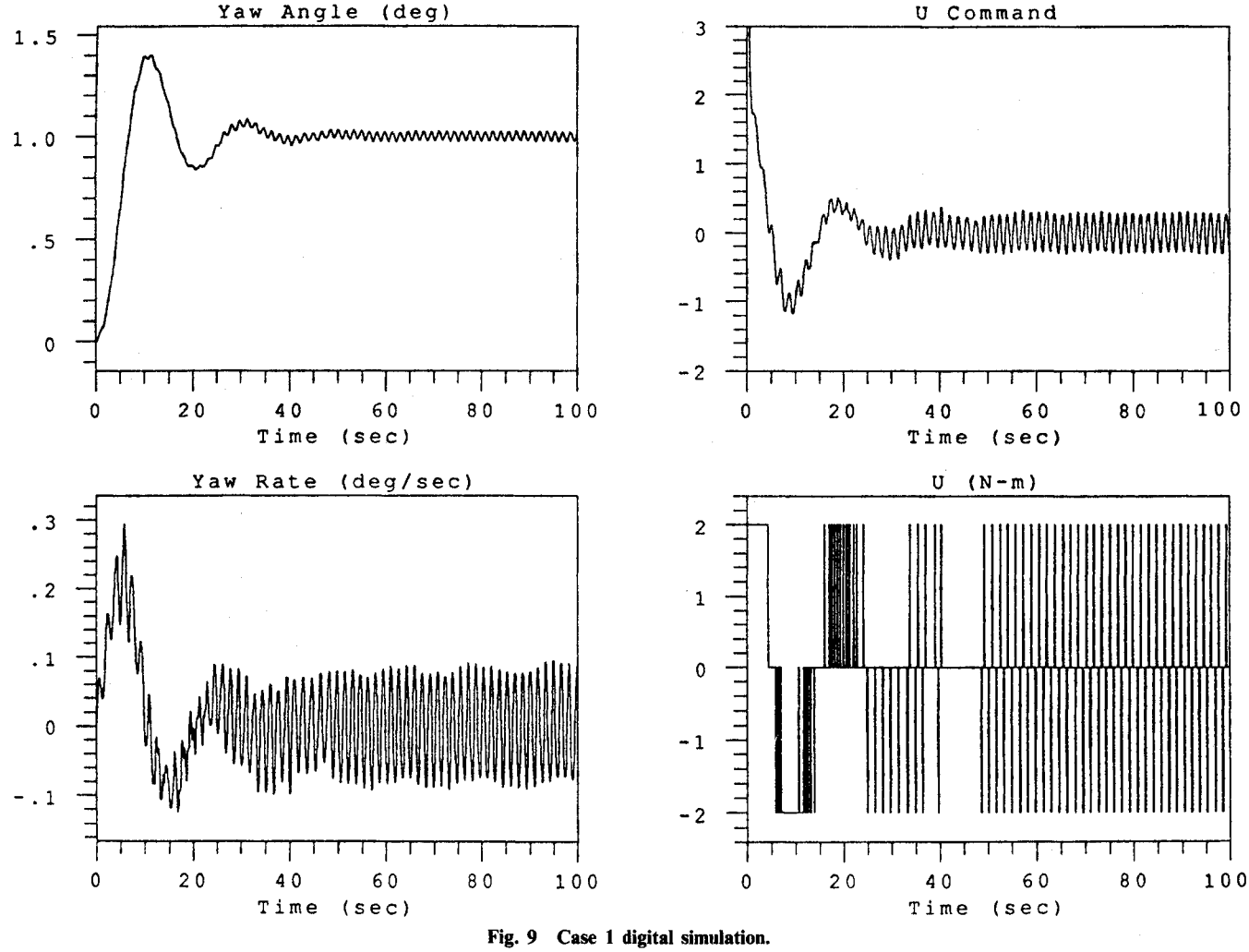

Fig. 9 Case 1 digital simulation.

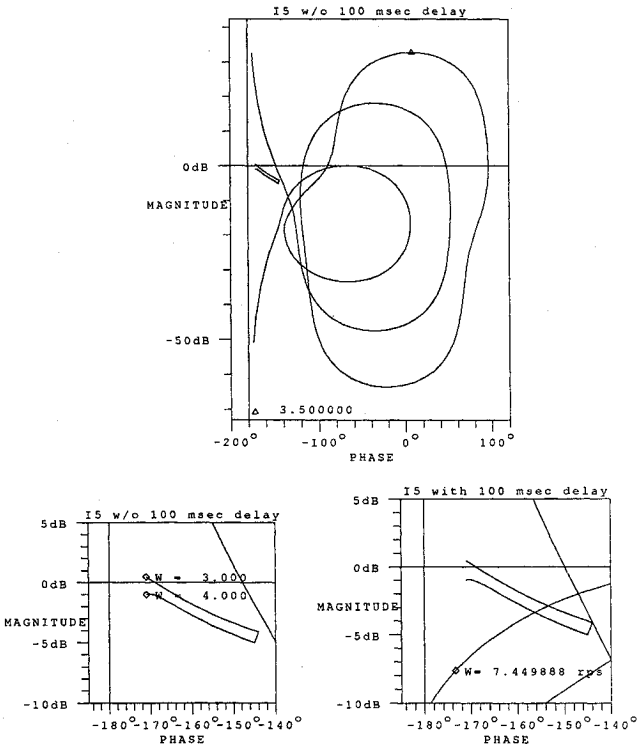

Fig. 10 Case 2 describing function analysis.

interaction of the pulse modulation with the flexible structural modes, was of primary concern for the INTELSAT 5 control system design; however, it will be shown that a robust nonlinear control system can be synthesized through use of classical linear compensation techniques.

Four different compensation schemes, consisting of different combinations of the phase-lead filters and structural filters, are discussed in this section. The filter parameters are given in Table 2. In case 1, the linear compensation consists of a lead filter without any structural filtering. The filter has the effect of phase stabilizing the rigid-body mode and the structural modes. Figure 8 contains several gain-phase plots; the leftmost plot shows the $G(j\omega)$ and $-1/N(X,\omega)$ loci. The spacecraft's three flexible modes are visible with portions of the $G(j\omega)$ locus in the vicinity of the $-1/N(X,\omega)$ locus. The frequencies of the upper and lower curves on the $-1/N(X,\omega)$ locus are 3 and 4 rad/s, respectively, which correspond to the frequency range of the dominant mode. The phase separation between the second mode and the minimum amplitude line of the $-1/N(X,\omega)$ locus is less than 15 deg.

A time delay is used to evaluate the phase margin of the control loop. By combining time delay model with the compensation, the $G(j\omega)$ locus can be shifted to the left, creating an intersection with the $-1/N(X,\omega)$ locus of the PWPF modulator. A second-order Padé approximation of a pure delay given by

$$e^{-Ts} = \frac{1-(Ts/2)+(Ts^2/12)}{1+(Ts/2)+(Ts^2/12)}$$

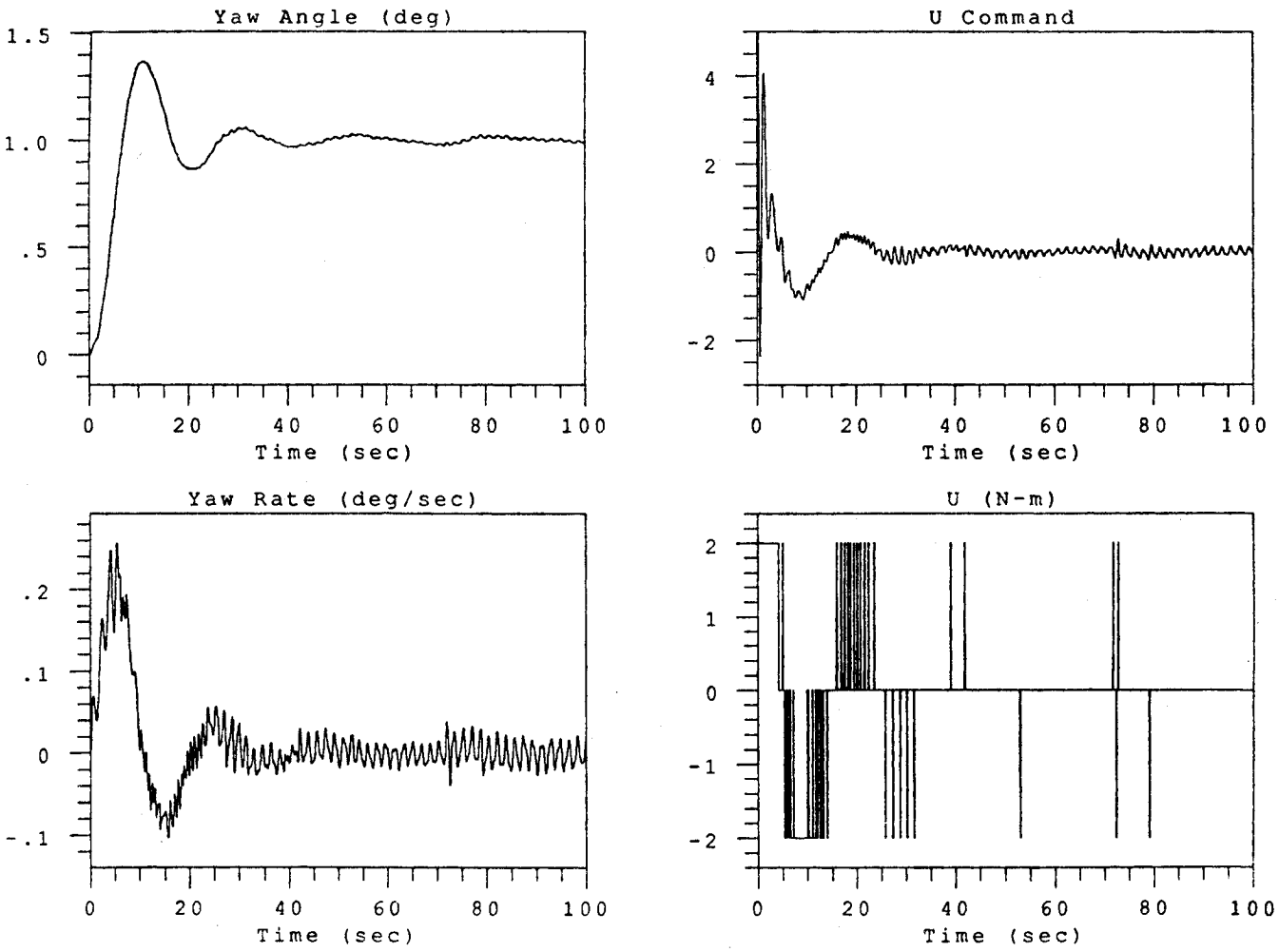

Fig. 11 Case 2 digital simulation.

is used, where the delay time T is found by the relation

$$T = \frac{\phi_m}{57.3\omega} \tag{27}$$

where ω (rad/s) is the frequency of the point of the $G(j\omega)$ locus close to the $-1/N(X,\omega)$ locus and ϕ_m is the phase margin in degrees. The smallest value of ϕ_m that causes an intersection is defined as the nonlinear phase margin. The lower right-hand plot depicts the introduction of a 100-ms delay at 3.5 rad/s; the corresponding phase lag, according to Eq. (27), is 20.1 deg. Note that the second mode now crosses the $-1/N(X,\omega)$ locus. The frequency of the $G(j\omega)$ locus near the describing function plot is close to 4 rad/s, making a limit cycle at that frequency possible. Note the nearly orthogonal crossing of the $G(j\omega)$ locus with the $-1/N(X,\omega)$ locus which, as mentioned previously, increases the accuracy of the describing function analysis.

Figure 9 shows the results of a nonlinear simulation of the case 1 compensation with the additional 100 ms delay. As predicted, a limit cycle is evident in all four states displayed in the figure. The rigid-body mode is sufficiently damped, but the second flexible mode experiences a structural limit cycle.

The nonlinear phase margin of the system with case 1 compensation is less than 15 deg, which may not prove sufficient in actual operation; increasing the nonlinear phase margin will further decrease the chance of structural limit cycling. This can be accomplished by introducing phase lead into the system. As a result, the case 2 compensation contains a phase-lead structural filter in addition to the lead filter for the rigid-body mode stabilization. A filter that would introduce significant phase lead between the frequencies of 3 and 4 rad/s was desired; the generalized structural filtering approach was employed to select the minimum-phase lead filter.[12] Figure 10 details the $G(j\omega)$ and $-1/N(X,\omega)$ loci for case 2. It can be seen that the nonlinear phase margin has roughly doubled from case 1 to 30 deg. Addition of the 100-ms delay does not result in an intersection between the curves; there is still a 10-deg phase difference between the $-1/N(X,\omega)$ and the $G(j\omega)$ loci. Therefore, no limit cycle is predicted from describing function analysis.

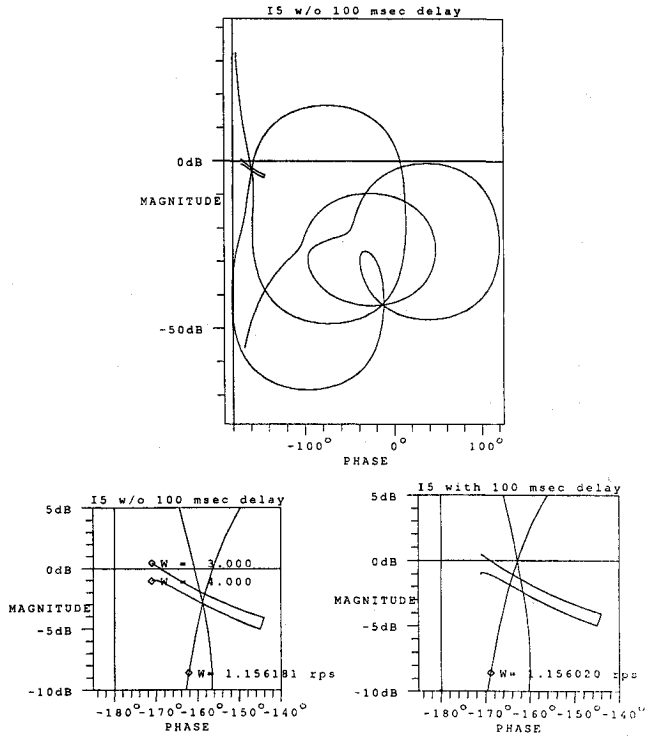

Fig. 12 Case 3 describing function analysis.

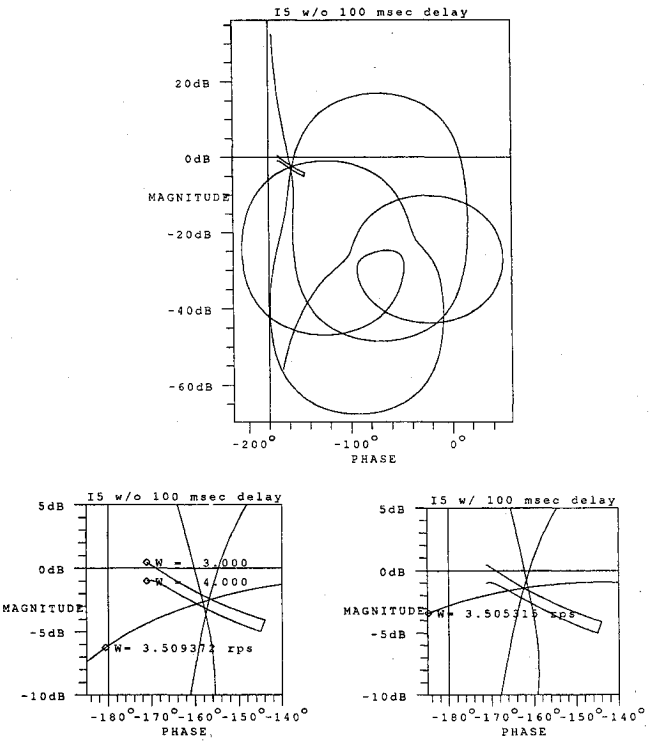

Fig. 13 Case 4 describing function analysis.

From Fig. 11, it can be seen that there is indeed no limit cycle; the yaw angle output contains gradually decreasing flexible mode excitation. No high-frequency thruster firings are evident; the low-frequency steady-state pulses that are visible depict the rigid-body mode limit cycle.

The case 2 compensation represents a method of phase stabilization of the nonlinear system; an alternative method of stabilization is gain stabilization. Along with the phase-lead filter from case 1, case 3 contains a minimum-phase notch filter. This notch filter provides a sharp gain attenuation at 3.4 rad/s. As evidenced by the mark in the right-hand plot in Fig. 12, there is a wide separation between the $-1/N(X,\omega)$ locus and the 3.5-rad/s point on the $G(j\omega)$ locus; as a result, the system has a large nonlinear phase margin. As predicted, the addition of the 100-ms delay does not provide enough phase lag to allow the curves to cross. The utility of the case 3 compensation is, however, misleading as a result of the wide phase margin apparent in the system. The disparaging phase characteristics of the notch filter undermine its suitability as a gain-stabilizing device. The case 4 compensation resembles the filters used in case 3 except that the notch filter pole and zero lie on the opposite side of the 3.5-rad/s mode. This demonstrates the effect of structural mode uncertainty on a control system. The notch filter is not an example of robust compensation because of the linear instability that could arise from structural pole or zero uncertainty; case 4 could represent an analogous situation in the nonlinear sense. As a result of the notch frequency mismatching, the $-1/N(X,\omega)$ and $G(j\omega)$ loci intersect as shown in Fig. 13.

Conclusions

A new way of using the describing function method for pulse-modulated control system design has been presented. Emphasis was given to the inherent modeling uncertainty of the describing function method. It was shown that if $-1/N(X,\omega)$ and $G(j\omega)$ loci intersect almost perpendicularly, the gain uncertainty for the pulse modulator does not prevent the use of the describing function method as a tool for predicting nonlinear instability. The INTELSAT 5 spacecraft was used as an example to demonstrate the concept and methodology developed in the paper.

Acknowledgments

This research was supported by NASA Marshall Space Flight Center under Contract NAS8-36224. The authors would like to thank Frank H. Bauer and John P. Downing of NASA Goddard Space Flight Center for their help and ideas for the framework of the describing function modifications in INCA.

References

[1]Kochenburger, R. J., "A Frequency Response Method for Analyzing and Synthesizing Contactor Servomechanisms," *AIEE Transactions*, Vol. 69, 1950, pp. 270–284.

[2]Gibson, J. E., *Nonlinear Automatic Control*, McGraw-Hill, New York, 1963, pp. 380–385.

[3]Gelb, A., and Vander Velde, W. E., *Multiple-Input Describing Functions and Nonlinear Design*, McGraw-Hill, New York, 1968, pp. 163–185.

[4]Ramos, A., "A Study of the Stability of the INTELSAT V SK Yaw Thruster Loop," COMSAT, Washington DC, SPLAB/77-1369, Dec. 1977.

[5]Wie, B., and Plescia, C., "Attitude Stabilization of Flexible Spacecraft During Stationkeeping Maneuvers," *Journal of Guidance, Control, and Dynamics*, Vol. 7, No. 4, 1984, pp. 430–436.

[6]Kubiak, E. T., Penchuk, A. N., and Hattis, P. D., "A Frequency Domain Stability Analysis of a Phase Plane Control System," *Journal of Guidance, Control, and Dynamics*, Vol. 8, No. 1, 1985, pp. 50–55.

[7]Bryson, A. E., *Control of Spacecraft and Aircraft*, Dept. of Aeronautics and Astronautics, Stanford Univ. Stanford, CA, 1987, pp. 34–39 (to be published as a textbook).

[8]DeBra, D. B., "Pulse Modulators," Class Notes, Dept. of Aeronautics and Astronautics, Stanford Univ., Stanford, CA, 1980.

[9]Golub, A. D., "OMV RCS Preliminary Control Loop Model and Gain Selection," TRW, Redondo Beach, CA, 87. L131.7-086, Nov. 1987.

[10]Bauer, F. H. and Downing, J. P., "Control System Design and Analysis Using Interactive Controls Analysis (INCA) Program," AIAA Paper 87-2515, Aug. 1987.

[11]Gibson, J. E., and Prasanna-Kumar, K. S., "A New RMS Describing Function for Single-Valued Nonlinearities," *Proceedings of the IRE*, Vol. 49, 1961, p. 321.

[12]Wie, B. and Byun, K. W., "A New Generalized Structural Filtering Concept for Active Vibration Control Synthesis," *Journal of Guidance, Control, and Dynamics*, Vol. 12, No. 2, 1989, pp. 147–154.